Available online at www.sciencedirect.com
ScienceDirect
Journal of the European Ceramic Society 29 (2009) 425–430
www.elsevier.com/locate/jeurceramsoc

Influence of crystal structure on crack propagation under cyclic electric loading in lead–zirconate–titanate

Ilona Westram [a], Hans Kungl [b], Michael J. Hoffmann [b], Jürgen Rödel [c,*]

[a] *WACKER SCHOTT Solar GmbH Carl-Zeiss-Str. 4, 63755 Alzenau, Germany*
[b] *Institut für Keramik im Maschinenbau Universität Karlsruhe, Haid-und-Neustr. 7, 76131 Karlsruhe, Germany*
[c] *TU Darmstadt, FG NAW, Petersenstrasse 23, 64287 Darmstadt, Germany*

Received 2 November 2007; received in revised form 26 May 2008; accepted 30 May 2008
Available online 30 July 2008

Abstract

Crack propagation under cyclic electric loading was studied in two non-commercial compositions of lead–zirconate–titanate and compared to earlier results from a commercial composition. These materials were chosen to provide a well-defined variation in crystal structure, ranging from rhombohedral to tetragonal, including a composition from the morphotropic phase boundary. The results are presented in terms of crack propagation as a function of various electric load amplitudes. While the crack propagation rates were of the same order of magnitude in all three compositions, fracture occurred in an either trans- or intergranular manner with crack extension either in the form of a singular crack, a microcrack zone or with extensive secondary cracking. These differences in crack propagation are discussed in the context of different piezoelectric material properties.

Keywords: PZT; Mechanical properties; Ferroelectric properties; Microstructure

1. Introduction

In general, there are several types of crack patterns, which can form depending on the microstructure of a material and the type of loading. For example, in brittle, unnotched materials subjected to thermal shock, the initial flaw size as well as the temperature difference affect the crack formation: above a critical temperature difference ΔT_c, shorter unstable crack paths and closer crack spacing occurs, while few large and deflected cracks propagate for $\Delta T < \Delta T_c$.[1,2]

A related strain incompatibility on a large scale occurs at electrode edges in piezoelectric ceramics.[3] In this case, the strain incompatibility between electrically active and inactive regions induces mechanical stresses in the material. Either straight or deflected cracks develop, depending on the width of the electrodes and the polarization state of the material.

Especially in functional materials like piezoelectric ceramics, crack formation and propagation are of interest, since the materials have a wide range of industrial applications.[4,5]

On a more local scale, strain incompatibility arises in piezoelectric ceramics due to cyclic electric loading, prompting cyclic crack propagation. The first general observations of this phenomenon were made in the mid-1990s.[6–8] Cao and Evans[6] observed that crack propagation only takes place in the direction perpendicular to a cyclic electric field and is dependent on the field amplitude. These observations were confirmed by Lynch et al.[7] who attempted to model the observed behaviour based on step-like domain switching. Shieh et al.[8] investigated two different compositions of lead–zirconate–titanate, a PZT-5H and a PLZT 8/65/35. They found the crack patterns to differ, with a narrow zone of intergranular cracks propagating in PZT-5H and a broad microcracked band in PLZT. Other work mainly addressed the field-dependence of crack propagation[9–12] and the effect of an additional static mechanical load in combination with electric cycling on crack propagation.[13]

Recently, the mechanism responsible for crack propagation under cyclic electric loading was identified.[14] Westram et al. subjected double-cantilever-beam specimens of PIC to cyclic electric loading of different field amplitudes and correlated the results with a finite element model taking into account nonlinear material behaviour. In the experiments, crack propagation was found to occur in different stages: an initial pop-in is followed

* Corresponding author. Tel.: +49 6151 16 6302; fax: +49 6151 16 6314.
E-mail address: roedel@ceramics.tu-darmstadt.de (J. Rödel).

0955-2219/$ – see front matter © 2008 Elsevier Ltd. All rights reserved.
doi:10.1016/j.jeurceramsoc.2008.05.050

by a period of steady-state crack propagation and thereafter a decrease of the crack growth rate. The pop-in phenomenon was further studied in Ref. [15] and also correlated to a finite element model.

While the mechanism for crack propagation under electric cyclic loading is now correlated to varying electric fields and varying strain on a mesoscopic level, the influence of local strain on the microscopic level as determined by crystal structure has not been investigated in detail as yet. In previous works, mostly just one material composition was studied and the exact material properties were not discussed in the context of the observed crack propagation behaviour. Therefore, this work is focussed on the crack propagation behaviour as a function of the crystal structure of the material. In lead–zirconate–titanate, crystal structure can be adjusted by the ratio of lead–zirconate to lead–titanate. In addition to a commercially available material close to the morphotropic phase boundary and therefore a partly tetragonal, partly rhombohedral crystal structure, two materials were specifically designed with a rhombohedral crystal structure and a predominantly tetragonal crystal structure.

In the discussion, the different material properties are related to differences observed in the experimental behaviour. Thus, a more general conclusion about the phenomenon of crack propagation under cyclic electric loading can be drawn.

2. Experimental procedure

Previously, crack propagation measurements had been conducted with PIC 151, a commercial material manufactured by PI Ceramic (Lederhose, Germany).[13–16] It is a lead–zirconate–titanate at the morphotropic phase boundary and doped with nickel and antimony. The results of the earlier work will be contrasted to new results obtained with two tailor-made compositions of lead–zirconate–titanate. Both of these were doped with 1 mol% lanthanum and 2 mol% strontium. One has a Zr:Ti ratio of 60:40 and therefore a rhombohedral crystal structure. It will be labelled "PZT-LS-R" for future reference. The second one has a Zr:Ti ratio of 52.5:47.5 and a predominantly tetragonal crystal structure. It will be labelled "PZT-LS-T". These specimens were received as blocks of 12 mm × 12 mm × 5.8 mm. They were first ground to a height of 5 mm and then cut into bars of 12 mm × 5 mm × 1.5 mm.

All bars were polished down to a 1 μm finish on one of their 12 mm × 5 mm sides. A thin layer of conducting silver was painted onto the 12 mm × 1.5 mm sides to enable electrical contact.

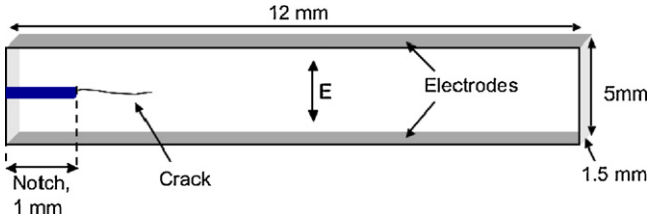

Fig. 1. Geometry of the specimens PZT-LS-R and PZT-LS-T. The electric field direction is indicated.

Thereafter, specimens were electrically poled at room temperature by applying a field of 2 MV/m across the 5 mm-direction for 20 min. Ferroelectric and strain hystereses were measured with an unnotched specimen of each material at a frequency of 0.01 Hz.

A 1-mm long through thickness notch was cut into one small side of the specimens using a diamond wire saw (4240, Well, Le Locle, Switzerland). The final specimen geometry is depicted in Fig. 1.

The experimental setup is the same as that used in previous works,[14,15] therefore a detailed description is omitted here. The frequency for the cyclic loading was 1 Hz.

After electrical cycling, pictures of the crack paths were taken with a CCD camera and the fracture surfaces were examined with a scanning electron microscope.

3. Results

The ferroelectric and strain hystereses of the three materials are depicted in Fig. 2. The materials differ slightly in their coercive field strengths as well as their strain.[17] The highest coercive field strength of $E_c = 1.2$ MV/m was observed in PZT-LS-T. In PIC 151, $E_c = 1$ MV/m, and in PZT-LS-R, $E_c = 0.8$ MV/m. At a field of 2 MV/m, PIC 151 displays the largest strain while PZT-LS-R displays the lowest.

In the crack propagation experiments, different electric field amplitudes were used. In order to facilitate comparison between the materials, the utilized field amplitudes were applied as multiples of the respective coercive field strength of the material.

Two specimens of each material were cycled at field amplitudes of 1.1/1.2/1.3/1.4 and 1.5 E_c, respectively. Furthermore, two specimens of the PZT-LS-T were cycled at 1.65 E_c and two

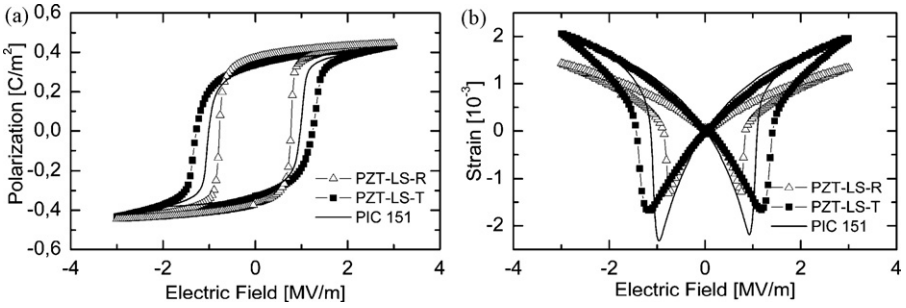

Fig. 2. (a) Ferroelectric hysteresis and (b) strain hysteresis for the three PZT compositions.

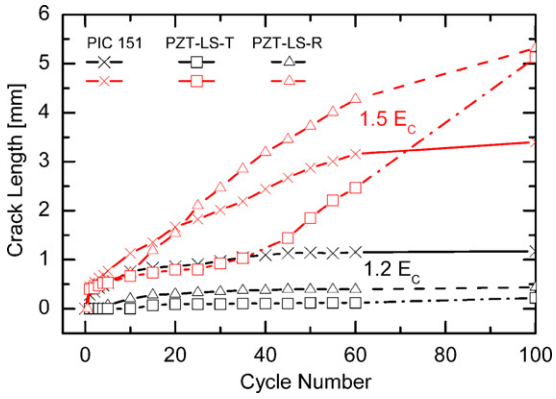

Fig. 3. Crack length vs. cycle number in all three PZT compositions for two different field amplitudes.

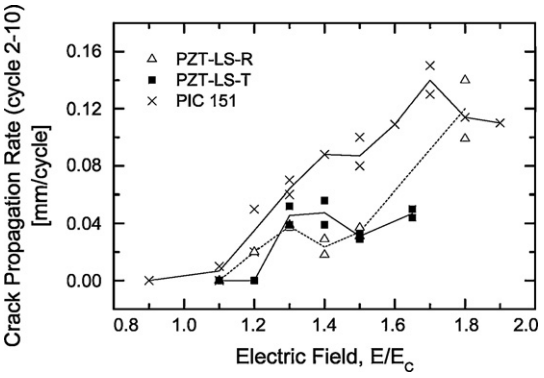

Fig. 4. Crack propagation rate during cycle numbers 2–10 as a function of the electric field amplitude in all three materials.

specimens of the PZT-LS-R were cycled at 1.8 E_c. 1.65 E_c was the highest field amplitude experimentally accessible in the case of PZT-L-T, since the coercive field strength was larger than in the other two compositions. The previously obtained results of PIC 151[14,16] are depicted in the figures below for comparison.

Fig. 3 provides a graph for crack length vs. cycle number, exemplarily for two different field amplitudes and the three materials. Clearly, the crack propagates further during the same number of cycles if the specimen is cycled at higher field amplitude. For 1.2 E_c, there is less than 1 mm of crack propagation even after 100 cycles in all materials. For 1.5 E_c, several millimeters of crack propagation take place within the first 60 cycles in PZT-LS-R and PIC 151. The crack length in PIC 151 is the highest up to approximately cycle number 20. Thereafter, the crack propagation rate gradually decreases, while crack propagation continues at a similar rate in PZT-LS-R. In PZT-LS-T, an incubation period can be discerned during which the crack propagation rate is low compared to the other two materials. However, the crack growth rate increases after the first 40 cycles, and finally, the crack in the PZT-LS-T specimen is as long as the crack in the PZT-LS-R specimen.

Intensive studies conducted previously on PIC 151 specimens[14–16] showed that crack propagation takes place in different stages: a pop-in event during the first polarization reversal is followed by a period of steady-state crack propagation and then a decrease of the crack growth rate. This decrease was usually accompanied by secondary cracking in PIC 151. Therefore, the crack propagation rates, which are displayed in Fig. 4 as a function of the field amplitude, were only evaluated for the first 10 cycles (excluding the pop-in). If secondary cracks are present, the crack propagation rate is difficult to assess, as several crack tips exist.

Fig. 4 quantifies the crack propagation rate, which increases with increasing field amplitude in PIC 151 and PZT-LS-R. In PZT-LS-T, this trend is not observed, which is presumably due to the incubation period. For cycle numbers larger than 10, a field-dependent crack propagation rate was also observed in PZT-LS-T. Fig. 4 also demonstrates that in the first 10 cycles, crack propagation in both PZT-LS materials only takes place for field amplitudes of 1.2 E_c and larger. This agrees with observations in PIC 151[14] and implies that large-scale domain switching is necessary to induce significant crack propagation.

Pictures of the crack paths in two specimens of each material taken after electrical cycling are provided in Fig. 5. The

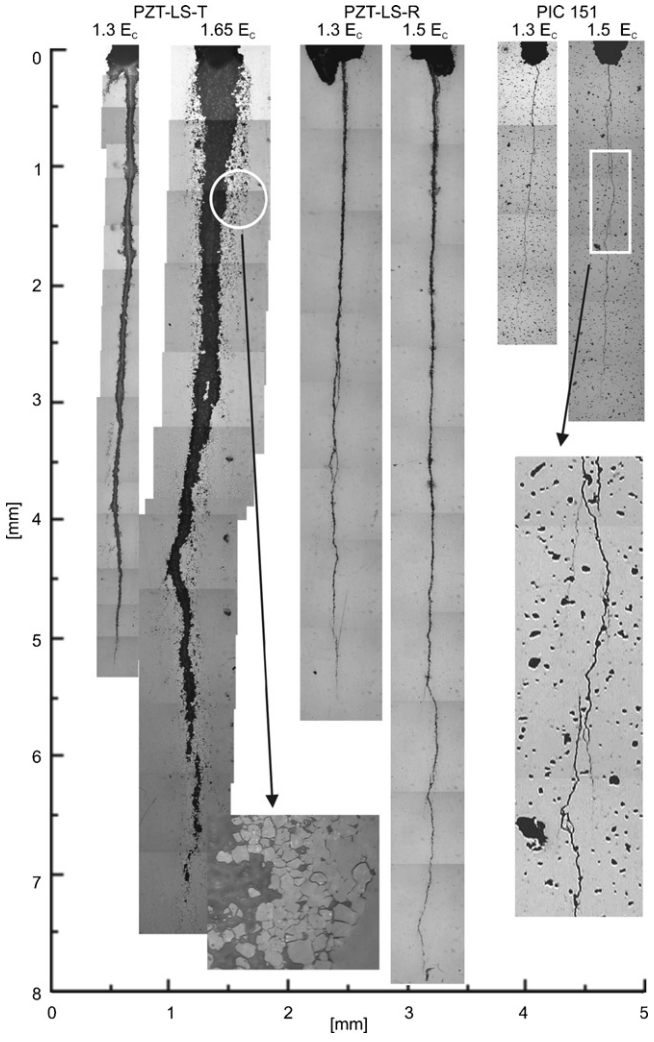

Fig. 5. Photographs of the crack paths in two specimens of each composition after electrical cycling with two different field amplitudes, respectively. Left: PZT-LS-T; center: PZT-LS-R; right: PIC 151. Magnified pictures are shown of the damage zone in PZT-LS-T and of the crack path in PIC 151.

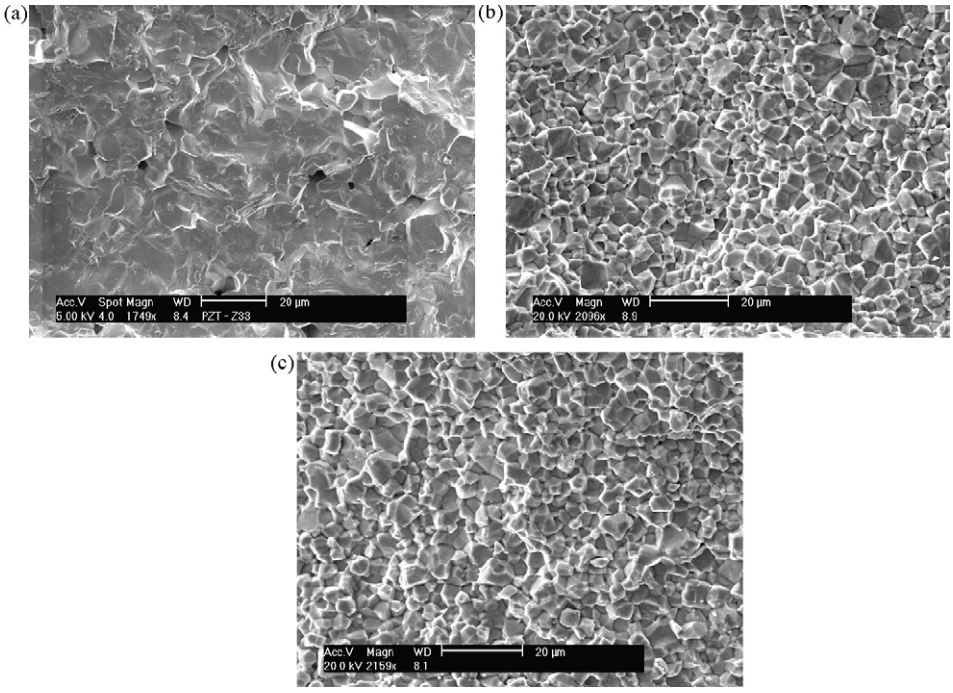

Fig. 6. Fracture surfaces in (a) PIC 151, (b) PZT-LS-R and (c) PZT-LS-T after electrical cycling.

appearance of the crack differs noticeably in all three materials. In PIC 151, secondary cracks were observed in nearly all specimens after as few as 10–50 cycles. In contrast, a damage zone around and in front of the crack occurred in PZT-LS-T with many microcracks. In PZT-LS-R, neither secondary cracking nor microcracks were observed with only one well-defined primary crack throughout the electrical cycling. These observations were consistent in all specimens cycled at different field amplitudes.

Differences between the materials were also observed in the fracture surfaces. While cracking was purely intergranular in both PZT-LS materials, mostly transgranular cracking occurred in PIC 151. This is seen in Fig. 6, where exemplary sections of the fracture surfaces of all three materials are shown. From these pictures, the grain size of both PZT-LS materials was determined to be around 4–5 μm, while the grain size of PIC 151 was found to be approximately 6–7 μm.

As summary, the material properties which were either known before this work or determined within this work, are listed in Table 1.

4. Discussion

The experimental results in this work show that all three different compositions of lead–zirconate–titanate display macroscopically similar crack propagation behaviour. Crack growth occurs perpendicular to the applied electric field and the crack propagation rates are of the same order of magnitude.

However, there are distinct differences in crack propagation rate, appearance of the crack path and of the fracture surfaces. This indicates that the material differences do affect the fracture behaviour to a certain extent. In principle, both the crack resistance behaviour as well as the electrical properties may

Table 1
Properties of the three different PZT compositions

Material composition	PIC 151	PZT-LS-T	PZT-LS-R
Crystal structure	MPB	Tetragonal	Rhombohedral
Lattice distortion (c/a: 1 in case of tetragonal crystal structure)	0.015[18] (tetragonal part)	0.022[19]	$9/8[(d_{111}/d_{-111})-1] = 0.007$[19]
Grain size	6–7 μm	4–5 μm	4–5 μm
Doping (mol%)	2.67 Ni, 5.33 Sb	2 La, 1 Sr	2 La, 1 Sr
Relative permittivity, poled	2400	1788	591
Coercive field strength (MV/m)	1.0	1.2	0.8
Total strain at 2 MV/m (10^{-3})	3.9	3.2	2.3
Remanent strain (10^{-3})	2.3	1.7	1.3
Polarization at 2 MV/m (C/m^2)	0.39	0.38	0.43
Remanent polarization (C/m^2)	0.33	0.34	0.37
Fracture mode	Transgranular	Intergranular	Intergranular
Crack path	Bifurcation	Damage zone	Single crack

be responsible. According to Glazounov et al.,[20] the tetragonal PZT material has a lower crack resistance and a lower R-curve and therefore would be expected to have a higher crack growth rate, in contradiction to our experimental observation. Thus, the different crack resistance between the three materials is not responsible for the observed behaviour. Further, fracture surfaces[8] and thus fracture mechanisms have been found to differ in electrically and mechanically driven crack propagation. Knowledge from mechanically driven crack growth, therefore, cannot be rigorously transferred to our situation. Hence, for the following discussion four material parameters appear important:

a) The total strain achievable governs the expected strain mismatch between different volumes around the notch or crack.[14]
b) On a microscopic scale, residual stresses result from the lattice distortion and will influence the crack path.
c) Grain boundary chemistry will play a role and will determine whether the grain or the grain boundary will crack.
d) The materials used exhibit a different permittivity, which influences the strain mismatch[14] between different volumes and hence the crack driving force.

First, we focus on the macroscopic crack propagation behaviour. In Ref. [14] the strain mismatch due to electric field inhomogeneities was identified to generate mechanical stresses, which are in turn responsible for crack propagation. For this reason, it would be expected that materials displaying different total strain display different magnitudes of crack propagation in terms of their crack propagation rates. This correlation between high strain and high-crack propagation rate has indeed before been observed by Weitzing et al.[9] Hence, the material with the largest strain amplitude, PIC 151, displays the largest crack propagation rates in the first 10 cycles. The higher mismatch in strain leads to a more extended range of high-stress intensity factor in front of the crack tip.[14] The PZT-LS-R material has the least strain mismatch and thus exhibits the lowest crack propagation rate in the first number of cycles.

Second, we consider the residual stresses on a microscopic scale. PZT-LS-R has the lowest lattice distortion and therefore the lowest microscopic residual stresses. These are suggested not to interfere with the macroscopic crack tip stress field and do not affect the crack path. Thus, there is only a single crack in PZT-LS-R. PZT-LS-T and PIC151 both have a higher level of local residual stresses and have the potential to lead to either microcracking or secondary cracking.

Third, grain boundary chemistry may affect, whether grain boundary or grain interior will crack. These differences have been observed before in a study of bipolar cycling of unnotched, bulk discs.[21] Both PZT-LS materials exhibit grain boundary cracking. Microcracking can thus occur for the material, which has high-local residual stresses (PZT-L-T). For the PIC151, microcracking in the grain interior is unlikely, however, secondary cracking due to the large stressed volume in front of the crack tip occurs.

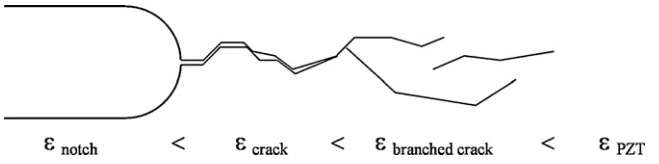

Fig. 7. Sketch of notch and different stages of crack propagation together with ranking of local relative permittivities.

Fourth, the differences in relative permittivities between the three materials affect the enhancement of electric field in front of the crack[22] and thereby influence the strain incompatibility between different volumes before and behind the crack tip.[14] PZT-LS-T and PIC151 differ only by 30% in relative permittivity, which is a small difference compared to other effects. The low permittivity of PZT-LS-R is suggested to be another reason for the low-crack propagation rate as compared to the other materials (at least in the first 10 cycles).

There is a secondary effect related to the permittivity, which can explain why the crack growth rate changes with crack extension. This happens only to a very limited degree with PZT-LS-R, but to a large degree with PIC151 (Fig. 3). For the discussion, consider a simple sketch of notch, pop-in and primary crack extending with the zone of secondary cracks further ahead of the notch (Fig. 7). The pop-in from the notch is comparable for all three materials (about 0.2–0.5 mm). The notch is a comparatively large, well defined, volume with a relative permittivity of the silicone oil of $\varepsilon_{notch} = 2.7$. It is much smaller than the relative permittivity of the PZT. Therefore, the notch is barely permeable to the electric field and the field lines bend around the notch and constitute a highly inhomogeneous field. This is consistent with the earlier observation that the pop-in from the notch is more pronounced than further crack propagation.[14] The crack provides us with a different scenario. A cyclic opening and closing of the crack, which was observed during the experiments, causes debris and wear of the fracture surfaces to mix with the silicone oil. A similar observation was made by Shieh et al. in PZT-5H.[8] Therefore, the permittivity of the crack is increased. In measurements with Kelvin Probe microscopy across the crack, a relative permittivity of approx. 40 was found which confirms this presumption.[23] This is one order of magnitude larger than the permittivity of the silicone oil, and the difference to the permittivity of the ceramic is not as large as in the case of the notch. Thus, the crack is more permeable for the electric field. Hence, the field distribution is less inhomogeneous and less strain mismatch results. The driving force for crack propagation is therefore lower than for the pop-in.

In the case of branched crack propagation, as in the case of PIC151, less strain mismatch is caused. A branched crack is even more permeable for the electric field, i.e. the average permittivity of this region is larger. Hence, the reduced crack propagation rate with increasing cycle number, particularly apparent with the PIC151, can be rationalized (Fig. 3). The different stages of crack propagation are schematically depicted in Fig. 7. With this simplistic picture, a realistic explanation of the observed behaviour can be provided.

5. Conclusions

1. Total achievable strain of the piezoceramic governs the crack propagation rate, at least in the initial stages of crack advancement.
2. The three different materials exhibit three types of crack propagation, single crack, microcrack damage zone and secondary cracking. This behaviour is related to their respective levels of residual stress (c/a – ratio) and to their tendency to exhibit either grain boundary cracking or cracking of the grain interior.
3. During crack propagation, the crack growth rate may slow down, due to a change of permittivity of the crack.

Acknowledgements

We thank the Deutsche Forschungsgemeinschaft (DFG) for supporting this work under contract number Ro 954/17. The excellent technical support by Emil Aulbach and Herbert Hebermehl is greatly appreciated.

References

1. Bahr, H.-A. and Weiss, H.-J., Heuristic approach to thermal shock damage due to single and multiple crack growth. *Theor. Appl. Fract. Mech.*, 1986, **6**, 57–62.
2. Pompe, W., Bahr, H.-A. and Weiss, H.-J., Thermal shock behaviour and crack pattern formation in brittle solids. In *Proceedings of the Conference Fracture Processes in Brittle Disordered Materials*, ed. J. G. M. van Mier. Chapman and Hall, London, 1991.
3. dos Santos e Lucato, S. L., Lupascu, D. C., Kamlah, M., Rödel, J. and Lynch, C. S., Constraint-induced crack initiation at electrode edges in piezoelectric ceramics. *Acta Mater.*, 2001, **49**, 2751–2759.
4. Uchino, K., *Piezoelectric Actuators and Ultrasonic Motors*. Kluwer, Boston, 1997.
5. Setter, N., ed., *Piezoelectric Materials in Devices*. Ceramics Laboratory EPFL, Lausanne, 2002.
6. Cao, H. and Evans, A. G., Electric-field-induced fatigue crack growth in piezoelectrics. *J. Am. Ceram. Soc.*, 1994, **77**, 17823–17886.
7. Lynch, C. S., Yang, W., Collier, L., Suo, Z. and McMeeking, R. M., Electric-field-induced cracking in ferroelectric ceramics. *Ferroelectrics*, 1995, **166**, 11–30.
8. Shieh, J., Huber, J. E. and Fleck, N. A., Fatigue crack growth in ferroelectrics under electrical loading. *J. Eur. Ceram. Soc.*, 2006, **26**, 95–109.
9. Weitzing, H., Schneider, G. A., Steffens, J., Hammer, M. and Hoffmann, M. J., Cyclic fatigue due to electric loading in ferroelectric ceramics. *J. Eur. Ceram. Soc.*, 1999, **19**, 1333–1337.
10. Zhu, T., Fang, F. and Yang, W., Fatigue crack growth in ferroelectric ceramics below the coercive field. *J. Mater. Sci. Lett.*, 1999, **18**, 1025–1027.
11. Liu, B., Fang, D.-N. and Hwang, K. C., Electric-field induced crack growth in ferroelectric ceramics. *Mater. Lett.*, 2002, **54**, 442–446.
12. Fang, D.-N., Liu, B. and Sun, C. T., Fatigue crack growth in ferroelectric ceramics driven by alternating electric fields. *J. Am. Ceram. Soc.*, 2004, **87**, 840–846.
13. Westram, I., Ricoeur, A., Emrich, A., Rödel, J. and Kuna, M., Fatigue crack growth law for ferroelectrics under cyclic electrical and combined electromechanical loading. *J. Eur. Ceram. Soc.*, 2007, **27**, 2485–2494.
14. Westram, I., Oates, W. S., Lupascu, D. C., Rödel, J. and Lynch, C. S., Mechanism of electric fatigue crack growth in lead zirconate titanate. *Acta Mater.*, 2006, **55**, 301–312.
15. Westram, I., Laskewitz, B., Lupascu, D. C., Kamlah, M. and Rödel, J., Electric-field induced crack initiation from a notch in a ferroelectric ceramic. *J. Am. Ceram. Soc.*, 2007, **90**, 2849–2854.
16. Westram, I., Crack Propagation in $Pb(Zr,Ti)O_3$ under Cyclic Electric Loading. Ph. D. Thesis, Darmstadt University of Technology, Darmstadt, Germany, 2006.
17. Hoffmann, M. J., Hammer, M., Endriss, A. and Lupascu, D. C., correlation between microstructure, strain behaviour and acoustic emission of soft PZT ceramics. *Acta Mater.*, 2001, **49**, 1301–1310.
18. Hackemann, S. and Pfeiffer, W., Domain switching in process zones of PZT: characterization by microdiffraction and fracture mechanical methods. *J. Eur. Ceram. Soc.*, 2003, **23**, 141–151.
19. Hoffmann, M. J. and Kungl, H., High strain lead-based perowskite ferroelectrics. *Curr. Opin. Solid State Mater. Sci.*, 2004, **8**, 51–57.
20. Glazounov, A. E., Kungl, H., Reszat, J.-T., Hoffmann, H. J., Kolleck, A., Schneider, G. A. and Wroblewski, T., Contribution from ferroelastic domain switching detected using X-ray diffraction to R-curves in lead zirconate titanate ceramics. *J. Am. Ceram. Soc.*, 2001, **84**, 2921–2929.
21. Balke, N., Kungl, H., Granzow, T., Lupascu, D. C., Hoffmann, M. J. and Rödel, J., Bipolar fatigue caused by field screening in $Pb(Zr\,Ti)O_3$ ceramics. *J. Am. Ceram. Soc.*, 2007, **90**, 3869–3874.
22. McMeeking, R. M., Electrostrictive stresses near crack-like flaws. *J. Appl. Math. Phys.*, 1989, **40**, 615–625.
23. Schneider, G. A., Felten, F. and McMeeking, R. M., The electrical potential difference across cracks in PZT measured by Kelvin probe microscopy and the implications for fracture. *Acta Mater.*, 2003, **51**, 2235–2241.